Sources, transport, and visibility impact of ambient submicrometer particle number size distributions in an urban area of central Taiwan

Li-Hao Young [a, *], Chih-Sheng Hsu [a], Ta-Chih Hsiao [b], Neng-Huei Lin [c], Si-Chee Tsay [d], Tang-Huang Lin [e], Wen-Yinn Lin [f], Chau-Ren Jung [g]

Supplemental Information

Table and Figure Captions:

Table S1. Summary statistics of the meteorological parameters and air quality during the study period.

Table S2. The bootstrap-estimated uncertainty of the input variables for each of the six PMF-resolved factors.

Table S3. The rotational uncertainty of the input variables for each of the six PMF-resolved factors.

Table S4. The temporal uncertainty of the input variables for each of the six PMF-resolved factors.

Fig. S1. A regional map depicting the study area and sampling sites (star: main site; circle: satellite site), and surrounding major stationary sources (diamond: power plant; square: steel plant; triangle: Taichung Port; hatched area: industrial or science park). The colored circle and shaded rectangle mark the Taichung urban basin and an area with a higher density of large emission sources, respectively. The right side of the map shows the highest and largest terrain in Taiwan, the Central Mountain Range.

Fig. S2. The size-dependent scaled measurement (counting) uncertainty (α_j) of the measured particle number size distribution.

Fig. S3. The distribution of the scaled residuals for the size-resolved particle number concentrations (n = size bins × hours = 531,647 data points).

Fig. S4. The average (solid line) and uncertainty (shaded area; expressed as ± one standard deviation) of the particle number size distribution profile for each factor.

Fig. S5. The diurnal variations in the total particle number, surface area, and volume concentrations for the six PMF-resolved factors.

Fig. S6. The non-parametric wind regression (NWR) plot for SO_2.

Fig. S7. The PMF-reconstructed aerosol extinction coefficient (b_p) versus the observed b_p.

Fig. S8. The distribution of trajectory densities for each season.

Fig. S9. The percentage of time, divided by season, that the study area was affected by the winds associated with each air-mass back trajectory cluster during the study period.

Table S1. Summary statistics of the meteorological parameters and air quality during the study period.

	Mean	SD	RSD
TEMP (ºC)	23.1	5.3	0.23
RH (%)	69.1	13.5	0.20
WS (m s^{-1})	1.5	0.7	0.48
UVI	1.4	2.3	1.69
PM_{10} (μg m^{-3})	35.2	21.6	0.61
CPM (μg m^{-3})	16.3	11.0	0.68
FPM (μg m^{-3})	20.3	13.2	0.65
SO_2 (ppb)	2.2	1.2	0.56
O_3 (ppb)	27.9	17.5	0.63
NO (ppb)	3.7	7.3	1.94
PN_{25} (cm^{-3})	7043	7208	1.02
$PN_{25\text{-}100}$ (cm^{-3})	6938	4890	0.70
$PN_{100\text{-}1000}$ (cm^{-3})	2365	1973	0.83
TPN (cm^{-3})	16347	11543	0.71

UVI: ultraviolet index; CPM: coarse particulate matter concentration (= PM_{10} – $PM_{2.5}$); FPM: fine particulate matter concentration ($PM_{2.5}$); PN: particle number concentration, where the subscript denotes the particle size range (in nm); and TPN: total particle number concentration.

Table S2. The bootstrap-estimated uncertainty of the input variables for each of the six PMF-resolved factors.

	F1	F2	F3	F4	F5	F6
TPN	1.0	0.1	0.1	0.8	0.5	0.2
TPS	0.1	0.1	0.3	0.2	0.4	0.3
TPV	0.1	0.1	0.5	0.1	0.3	0.4
CPM	0.4	0.9	1.0	0.9	1.3	1.1
FPM	0.0	0.5	0.4	0.0	0.8	1.0
b_{sp}	0.0	0.6	1.0	0.0	1.3	1.5
b_{ap}	0.4	0.5	1.0	0.5	1.3	1.7
SO_2	0.4	0.6	0.7	0.3	0.9	0.8
O_3	0.8	0.8	0.8	0.9	0.0	0.8
NO	0.8	1.2	1.0	0.7	0.8	0.0
RH	0.4	0.6	1.0	0.0	0.9	0.0
WS	0.6	0.7	0.9	0.6	0.9	0.8
UVI	1.3	1.5	0.0	2.0	1.9	2.0

The numbers are one standard deviations of the factor contributions (in %) for each input variable.

Table S3. The rotational uncertainty of the input variables for each of the six PMF-resolved factors.

	F1	F2	F3	F4	F5	F6
TPN	0.9	0.2	0.1	0.6	0.1	0.1
TPS	0.1	0.1	0.3	0.1	0.1	0.4
TPV	0.0	0.1	0.3	0.0	0.1	0.4
CPM	0.0	0.1	0.2	0.1	0.0	0.2
FPM	0.0	0.0	0.2	0.0	0.1	0.3
b_{sp}	0.0	0.0	0.2	0.0	0.2	0.4
b_{ap}	0.0	0.0	0.3	0.1	0.2	0.4
SO_2	0.1	0.1	0.1	0.1	0.0	0.1
O_3	0.1	0.1	0.0	0.1	0.0	0.1
NO	0.3	0.1	0.0	0.3	0.1	0.0
RH	0.2	0.3	0.1	0.0	0.0	0.0
WS	0.1	0.1	0.1	0.1	0.1	0.0
UVI	0.3	0.1	0.0	0.5	0.0	0.0

The numbers are one standard deviations of the factor contributions (in %) for each input variable.

Table S4. The temporal uncertainty of the input variables for each of the six PMF-resolved factors.

	F1	F2	F3	F4	F5	F6
TPN	16.4	5.9	3.0	11.4	13.5	8.4
TPS	4.3	5.6	17.3	6.6	13.3	14.8
TPV	3.2	7.2	22.9	3.0	11.4	16.7
CPM	2.0	20.7	14.3	7.9	9.8	10.8
FPM	0.0	20.7	19.2	0.0	11.3	12.1
b_{sp}	0.0	18.9	22.6	0.0	10.8	12.5
b_{ap}	4.2	11.2	14.3	5.0	15.5	12.0
SO_2	7.4	22.8	10.9	2.5	16.2	6.0
O_3	6.9	19.3	0.0	8.0	0.0	8.0
NO	13.9	21.8	14.9	4.5	13.2	0.0
RH	4.6	25.1	13.3	0.0	18.4	0.0
WS	9.5	22.8	7.0	5.7	9.7	0.0
UVI	14.0	23.0	14.8	6.5	4.8	0.0

The numbers are one standard deviations of the factor contributions (in %) for each input variable.

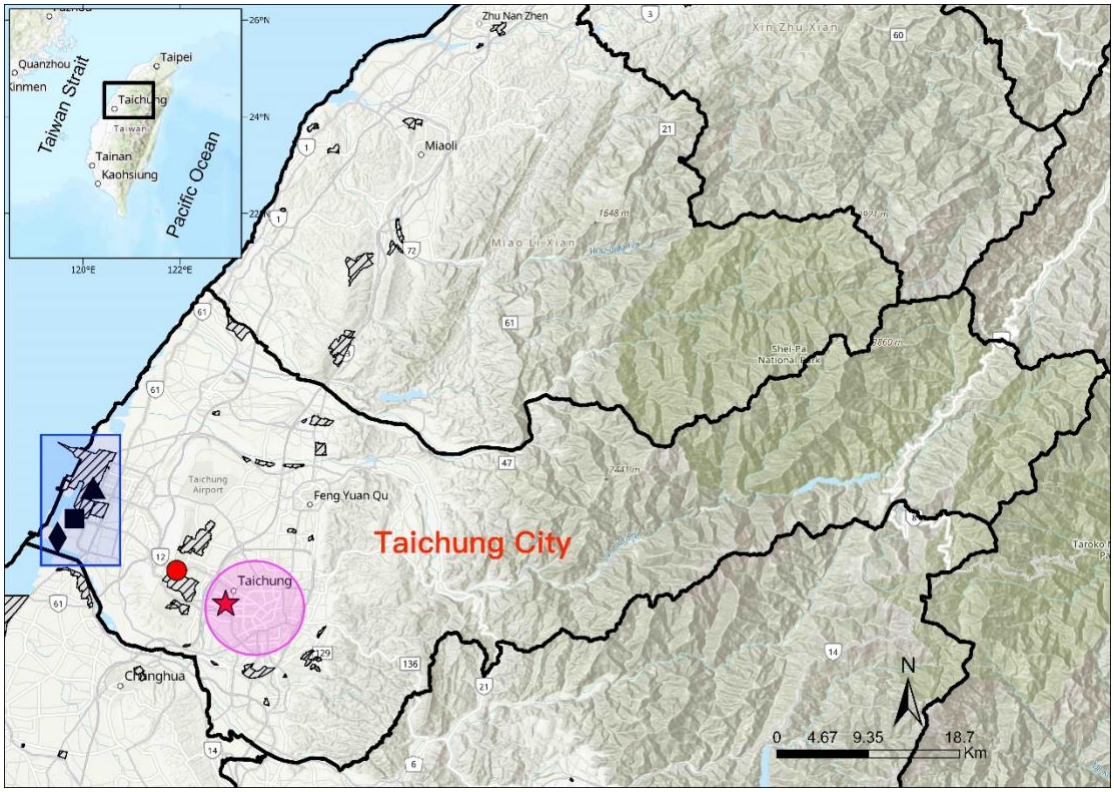

Fig. S1. A regional map depicting the study area and sampling sites (star: main site; circle: satellite site), and surrounding major stationary sources (diamond: power plant; square: steel plant; triangle: Taichung Port; hatched area: industrial or science park). The colored circle and shaded rectangle mark the Taichung urban basin and an area with a higher density of large emission sources, respectively. The right side of the map shows the highest and largest terrain in Taiwan, the Central Mountain Range.

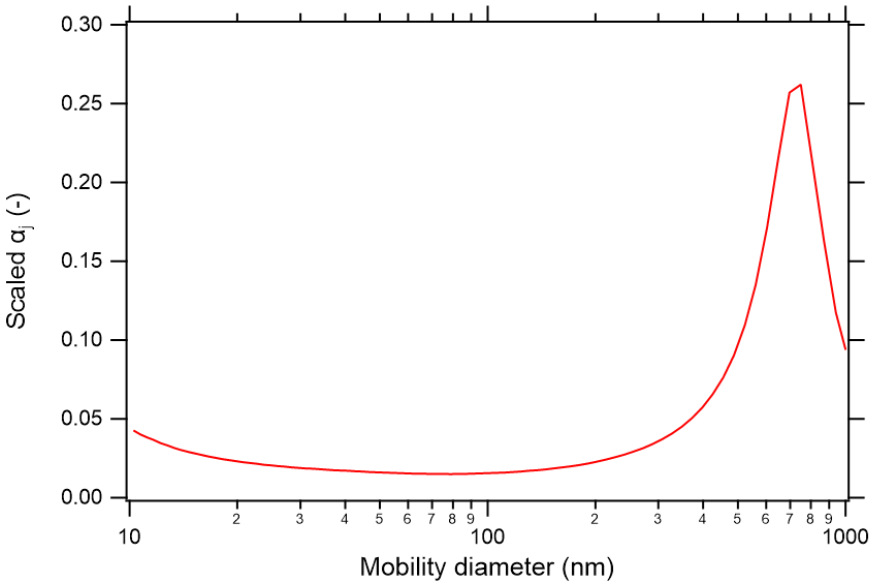

Fig. S2. The size-dependent scaled measurement (counting) uncertainty (α_j) of the measured particle number size distribution.

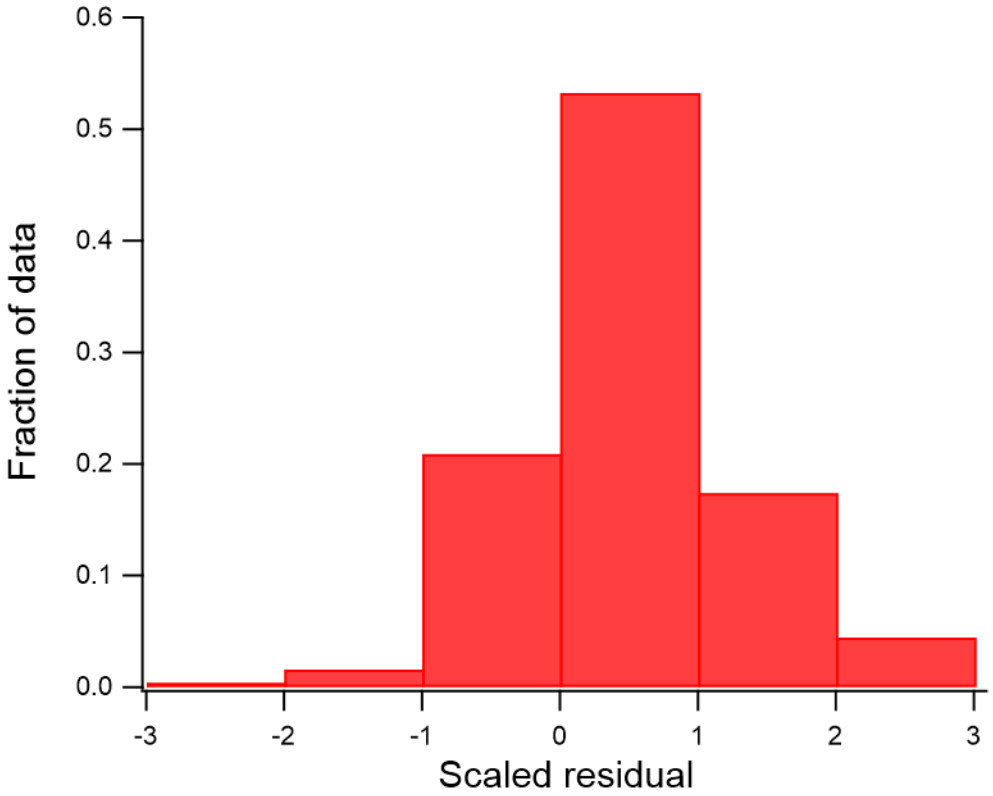

Fig. S3. The distribution of the scaled residuals for the size-resolved particle number concentrations (n = size bins × hours = 531,647 data points).

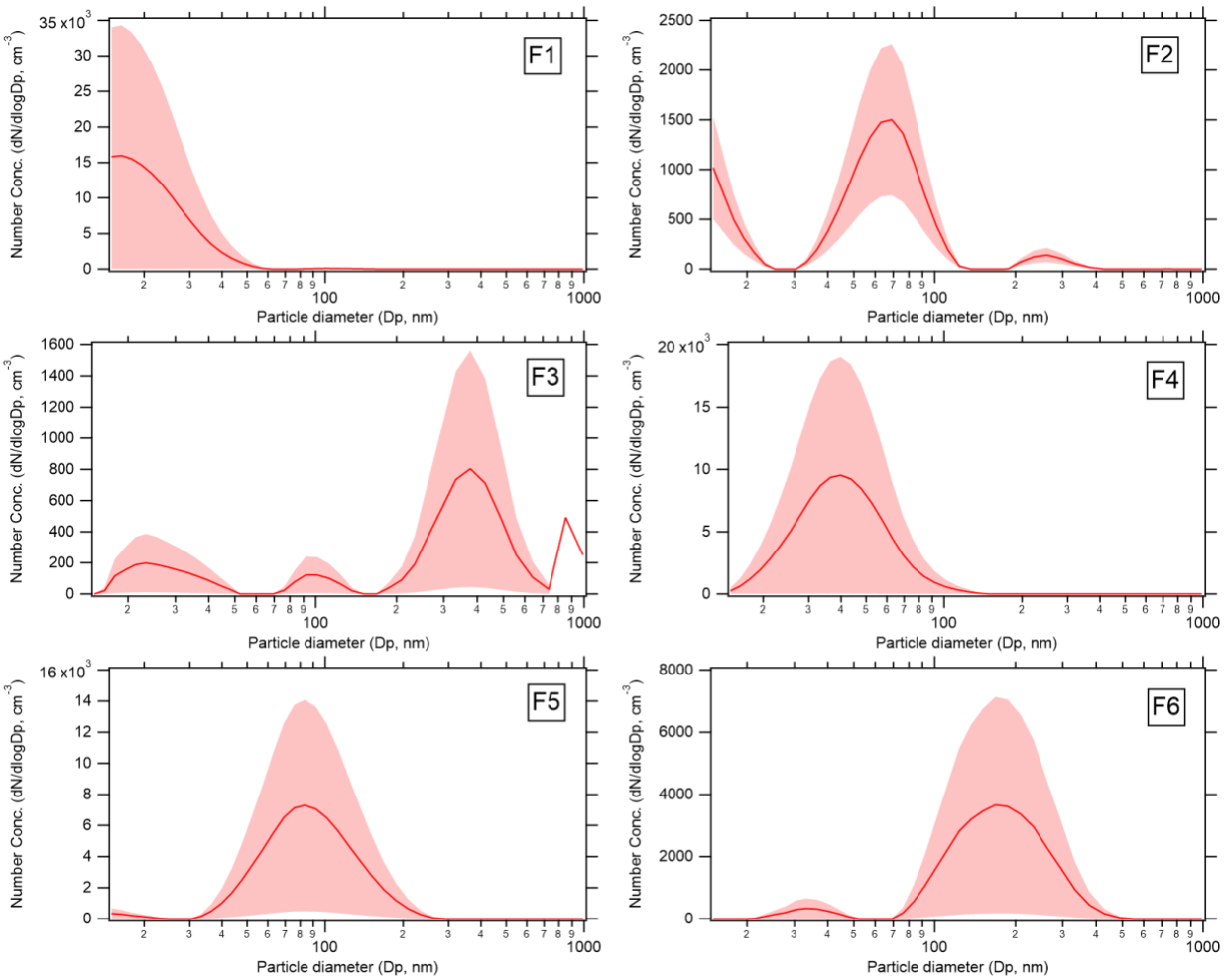

Fig. S4. The average (solid line) and uncertainty (shaded area; expressed as ± one standard deviation) of the particle number size distribution profile for each factor.

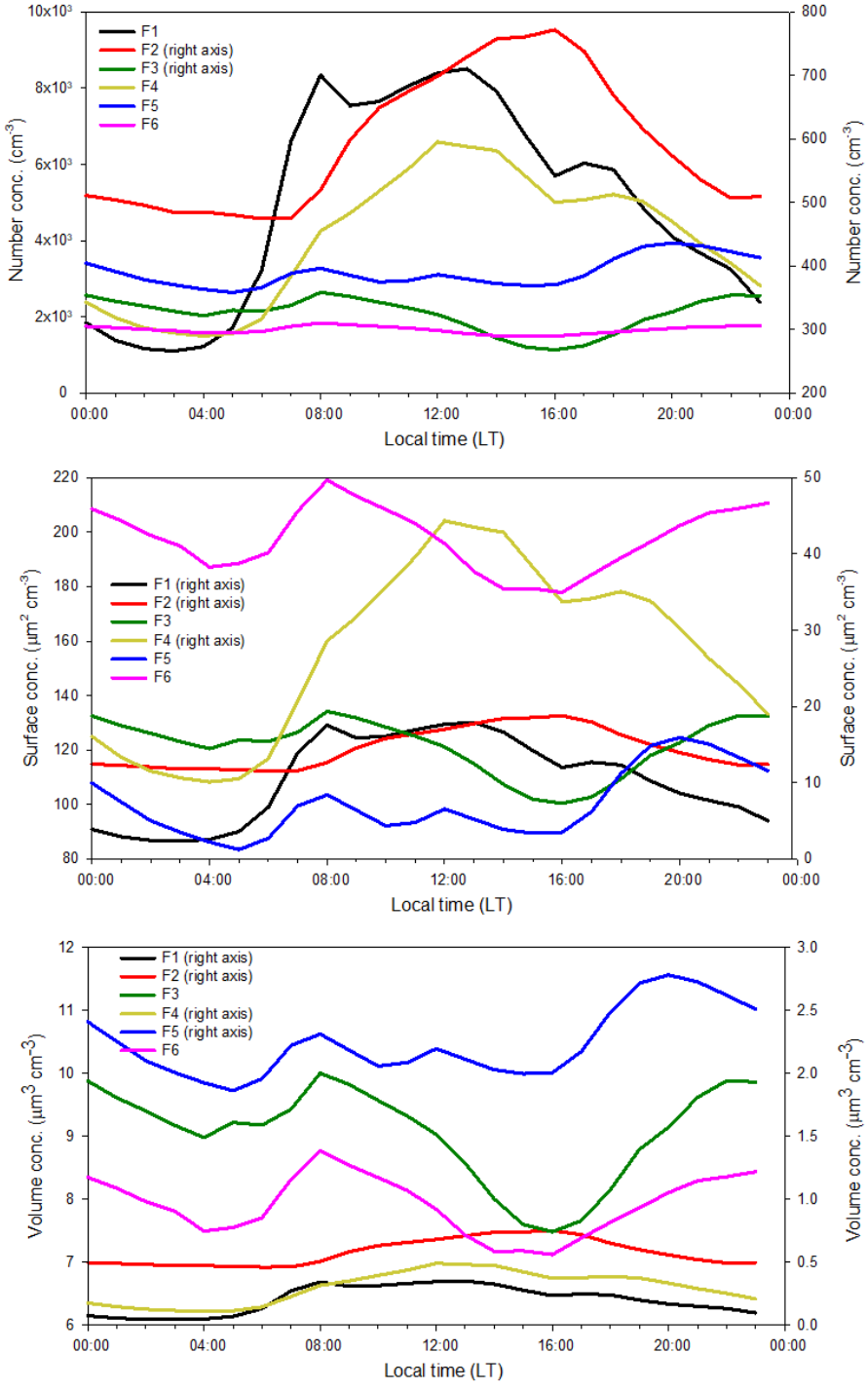

Fig. S5. The diurnal variations in the total particle number, surface area, and volume concentrations for the six PMF-resolved factors.

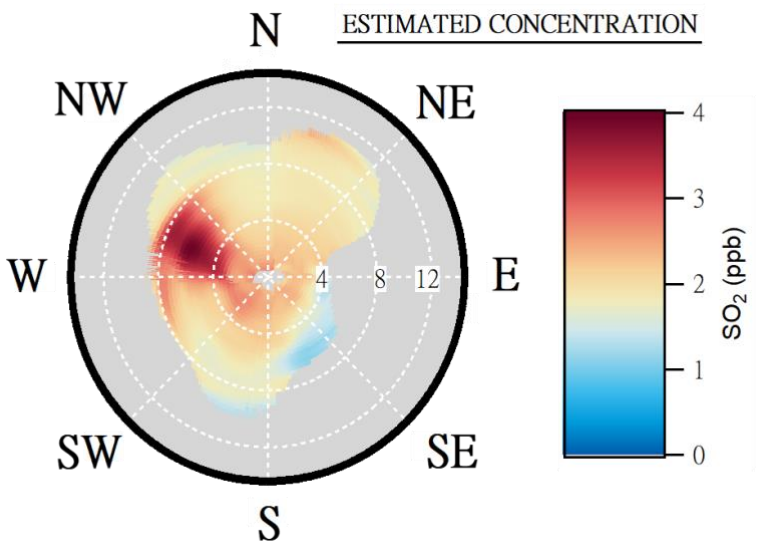

Fig. S6. The non-parametric wind regression (NWR) plot for SO_2.

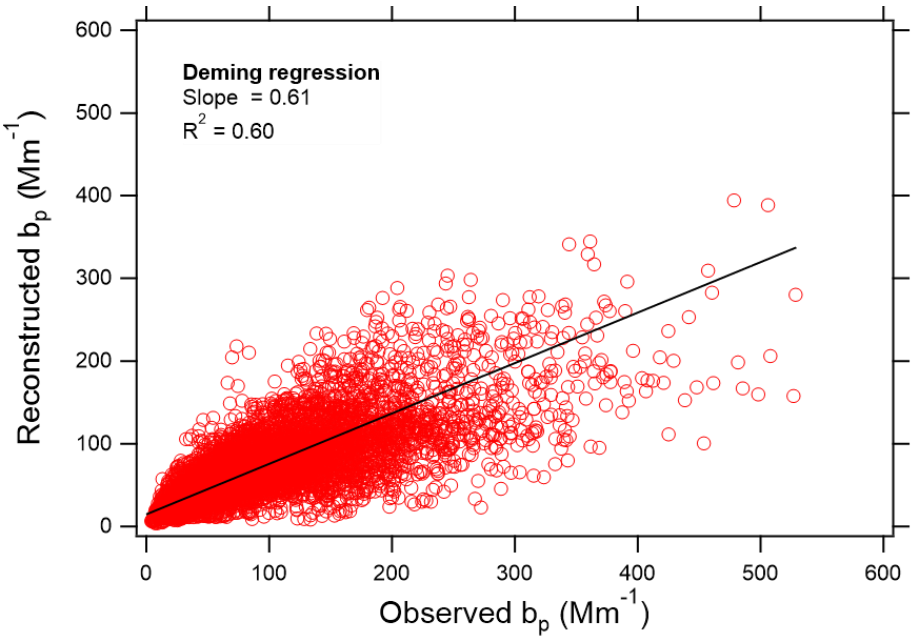

Fig. S7. The PMF-reconstructed aerosol extinction coefficient (b_p) versus the observed b_p.

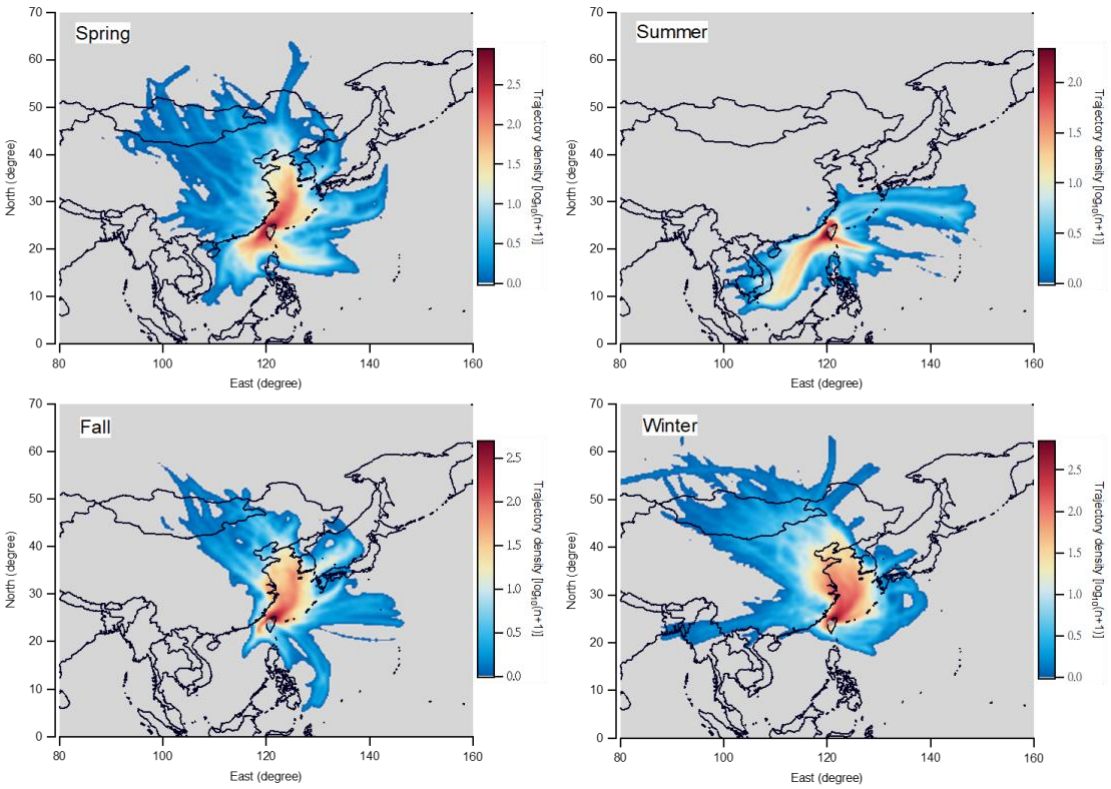

Fig. S8. The distribution of trajectory densities for each season.

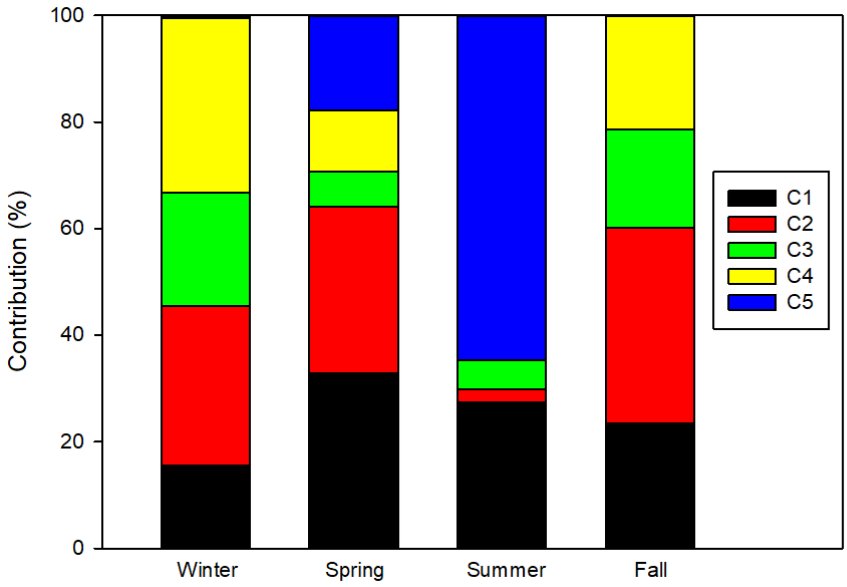

Fig. S9. The percentage of time, divided by season, that the study area was affected by the winds associated with each air-mass back trajectory cluster during the study period.